Unified theoretical description of out-of-equilibrium electron intraband dynamics in gold induced by femtosecond laser pulses

Stéphane Coudert,[1,2] Stefan Dilhaire,[3] Philippe Lalanne,[4] and Guillaume Duchateau[1,2,*]

[1]*CEA-CESTA, 15 Avenue des Sablières, CS60001, 33116 Le Barp Cedex, France*

[2]*Université de Bordeaux-CNRS-CEA, Centre Lasers Intenses et Applications - CELIA, 33405 Talence, France*

[3]*Laboratoire Onde et Matière d'Aquitaine (LOMA), UMR 5798, CNRS-Université de Bordeaux, 33400 Talence, France*

[4]*Laboratoire Photonique, Numérique et Nanosciences (LP2N), UMR 5298, CNRS-IOGS-Université de Bordeaux, Institut d Optique d Aquitaine, 33400 Talence, France*

(Received 22 July 2022; revised 5 October 2022; accepted 18 October 2022; published 25 October 2022)

The modeling of the intraband dynamics of conduction electrons in gold induced by a femtosecond laser pulse is addressed. Current approaches, based on the numerical resolution of the Boltzmann equation, are only able to describe electron excitation *or* relaxation processes. In the present paper, within a single formalism, our kinetic model accounts quantitatively for both excitation and relaxation processes, i.e., photon absorption, thermal conductivity, and electron-phonon coupling coefficient. We suggest that such an approach can only be built by including Umklapp processes in the description of electron collisions. In addition to normal electronic collisional processes with phonons and other electrons, the present theoretical description further includes these mechanisms: (i) a conduction electron can be scattered in the second Brillouin zone after a collision, contributing significantly to the photon absorption, and (ii) the influence of the discrete and periodic nature of the lattice on electron collisions is considered, enabling in particular the coupling between electron and transverse phonons. A good agreement of predictions of this unified modeling with experimental observations for absorption and energy transfer from electrons to the lattice is obtained. We have investigated the influence of the Umklapp processes on the imaginary part of the dielectric function, the electron-phonon coupling parameter, and the transient shape of the electron energy distribution.

DOI: 10.1103/PhysRevB.106.134308

I. INTRODUCTION

The ultrafast out-of-equilibrium electron dynamics in gold induced by femtosecond laser pulses has been studied for several decades, see for instance [1–4]. Experimental observations based on femtosecond pump-probe experiments have evidence a ∼100 fs out-of-equilibrium dynamics of photoexcited conduction electrons due to intraband transitions [3,5,6]. To understand this transient electron dynamics, kinetic approaches based on solving the Boltzmann equation have been developed [5,7]. By describing microscopic interaction processes, such an approach also allows calculating macroscopic properties of materials including the electron-phonon coupling constant (driving the energy transfer from electrons to the lattice) and thermal conductivity used in the so-called two-temperature model [8–10]. By providing an accurate description of the ultrafast out-of-equilibrium electron dynamics in materials, this kinetic approach is also an efficient tool for application purposes including photovoltaic devices and hot carriers photocatalysis [11–15], which efficiency may depend in general on both the time-dependent amplitude and shape of the electron energy distribution.

For photon energies below ∼1.9 eV and moderate laser intensities, the conduction electron dynamics mainly consists of excitation and relaxation processes through intraband transitions driven by electron collisions. For excitation, electrons gain energy due to photon absorption (where a third particle, a phonon or an electron, is involved for momentum conservation). The absorption is related to the imaginary part of the dielectric function. Regarding relaxation, it is due to electron collisions with phonons or other electrons (photons are not involved). Electron-electron collisions mainly leads the electron energy distribution to equilibrate towards the Fermi-Dirac statistics. Electron-phonon collisions are responsible for the energy transfer from electrons towards the lattice. Electron-phonon collisions also mainly drive the electron transport and heat transfer.

Various theoretical approaches have been developed to describe such a laser induced electron dynamics in gold. Models based on *ab initio* calculations [2,9,11,16,17] and semianalytic free electrons models [18,19] have been developed. *Ab initio* calculations give a very accurate and quantitative description of electron dynamics but require a large computational cost. Semianalytic approaches based on the free electron approximation are much more efficient and due to their relative simplicity, enable to get a good understanding of physical processes at play. For instance, in the paper of Blumenstein *et al.* based on a semianalytic approach [20], the intraband absorption has been considered by using a Drude model to compute optical properties accounting for electron temperature. However this approach considers electrons

*Corresponding author: guillaume.duchateau@cea.fr

at equilibrium. Kinetic approaches, accounting for out-of-equilibrium conditions, have been shown to be able to account for results of 100-fs-resolution pump-probe experiments in case of irradiation of nano objects [3,4,18,21]. Based solely on normal scattering processes (in the first Brillouin zone), electron relaxation including electron-electron scattering and electron-phonon coupling were correctly described. It follows that electron thermalization (transition to equilibrium) and electron energy transfer to the lattice (two-temperature model), respectively, are well described and allow to make comparisons to experimental data. However, such approaches cannot in the same time account for laser absorption and thermal conduction coefficients (which depends on electron-phonon collision frequency), i.e., they do not quantitatively account for both excitation and relaxation processes. In particular absorption is underestimated by one order of magnitude compared with experimental data (see results below).

The present paper aims at providing an unified kinetic description of both excitation and relaxation processes, including absorption, thermal conductivity, and electron-phonon coupling parameter for energy transfer from electrons to the lattice. We suggest that such an approach can only be built by including Umklapp processes in the description of electron collisions with another electron or phonon [electron scattering out of the first Brillouin zone (BZ1)]. We show that two kinds of Umklapp processes have to be included in this unified theoretical description. (i) An electron can simply be scattered by a phonon or an other electron in the second Brillouin zone (BZ2), contributing significantly to the photon absorption. The latter (Umklapp photon-electron-photon process) has been pointed out by [22] as being an important photon absorption process at optical frequencies. (ii) The second kind of Umklapp collision is due to the discrete and periodic nature of the lattice. This process enables in particular the coupling between electron and transverse phonons as shown for aluminum [10]. Such Umklapp processes are implicitly taken into account in *ab initio* formalism but due to its relative simplicity, our model highlights the specific role of such processes in absorption and relaxation processes being computationally efficient.

This paper is organized as follows. In Sec. II, the Boltzmann equation, which enables to model the laser induced femtosecond out-of-equilibrium electron dynamics is presented. The general formalism describing the various collisional processes (electron-electron and electron-phonon collision within an external electric field) is provided. The description of normal processes is recalled in Appendix A as it is used as a support for Umklapp theoretical description. The theoretical description of Umklapp processes requires computationally expansive simulations. In order to provide a relatively simple approach allowing fast and accurate description of the ultrafast out-of-equilibrium electron dynamics in gold for above mentioned application purposes, and to improve the understanding of the influence of Umklapp processes on the electron dynamics, a simplified approach is proposed. The latter is shown to capture the main influences of Umklapp processes, which can be split into two contributions. They are presented and the associated theoretical descriptions are detailed. In Sec. III, the numerical results obtained with the present approach are presented. Optical and thermal properties of gold (intraband optical permittivity, electron-phonon coupling constant, and thermal conductivity) are calculated. A good agreement with experimental values is obtained. The influence of each Umklapp process on the macroscopic observables is discussed. The first kind of Umklapp process is shown to mainly change the photon absorption efficiency, whereas the second kind is shown to have an influence on thermal conductivity and on the electron-phonon coupling constant. This good agreement and understanding of contribution of various processes to metal properties validate our approach. Finally main conclusions of this paper are drawn in Sec. IV. For the reader's convenience, Appendices provide some details on analytical calculations.

II. MODEL

The above mentioned unified theoretical approach aiming at modeling the femtosecond out-of-equilibrium electron dynamics in gold is presented in this section. The kinetic formalism consisting in solving the Boltzmann equation for electrons is introduced in Sec. II A, including a general description of collision operators. The collisional operators for normal processes (electron scattering in BZ1), hereafter referred to as N processes, has been widely studied over the past decades [5,10,18,23,24]. Nevertheless, as their description is the keystone for the understanding of our model for Umklapp processes, they are recalled in Appendix A. The Umklapp processes can be split into two classes pertaining to different interaction mechanisms. The first class, described in Sec. II B, corresponds to the electron scattering by a perturbation (phonon or other electron) towards BZ2. This mechanism is hereafter referred to as U_1 process. The second class of Umklapp process is presented in Sec. II C. It consists of a description of the electron-phonon interaction accounting for the discrete feature and periodicity of the lattice. The latter mechanism is hereafter referred to as U_2 process.

A. Kinetic description

1. Boltzmann equation

The description of the laser induced electron dynamics is done by solving the Boltzmann equation, which provides the evolution of the electron energy distribution, following a procedure similar to [5,18]. Assuming that the photon energy is below the interband threshold ($\hbar\omega < 1.9$ eV in gold), only the dynamics of free carriers in the conduction band can be described. This kinetic approach is reliable because the number of considered particles $\mathcal{N}$ is large enough in metals. The characteristic density of conduction electrons is $n_e \approx 10^{22}$ cm^{-3}, the laser focal spot size is $S \approx 1\ \mu$m^2, and the skin depth is $l_p \approx 10$ nm, leading to $\mathcal{N} \approx n_e \times S \times l_p \approx 10^{12}$, which is large enough to describe electrons by their energy distribution. Regarding the transport term of the Boltzmann equation, which accounts for thermal diffusion, it is not included in the present paper since we are only interested in deriving the main physical quantities driving the electron dynamics as presented in Sec. I (not to simulate the laser induced electron transport). Note this approach is compatible with the determination of the transport coefficient, which is related to the collision frequency and associated collision operators, which

are introduced below. The Boltzmann equation thus reads

$$\frac{\partial f(\mathbf{k})}{\partial t} = \left.\frac{\partial f}{\partial t}\right|_{e-pt-phL} + \left.\frac{\partial f}{\partial t}\right|_{e-pt-phT} + \left.\frac{\partial f}{\partial t}\right|_{e-pt-e} \quad (1)$$

where $f(\mathbf{k})$ stands for electron distribution function. $\mathbf{k}$ is the crystalline momentum of conduction electrons. The terms of the right-hand side of Eq. (1) are the collision operators including interactions between electrons (e), phonons (ph), and photons (pt). $\frac{\partial f}{\partial t}|_{e-pt-phL}$ and $\frac{\partial f}{\partial t}|_{e-pt-phT}$ account for the electron-photon-phonon interaction considering longitudinal (L) and transverse (T) phonons, respectively. They describe the absorption of photons assisted by a phonon (which ensures the total momentum conservation) [16], and are calculated with the usual procedure developed in [25]. When the laser electric field is zero, these collision operators reduce to the standard electron-phonon collision only leading to electron relaxation (mainly phonon emission by electrons). Hereafter, for the sake of conciseness, if the nature of phonons (L or T) is not mentioned, they are implicitly only longitudinal for normal processes and, longitudinal and transverse for Umklapp processes. $\frac{\partial f}{\partial t}|_{e-pt-e}$ accounts for the possible absorption of photons during an electron-electron collision. As shown below, this mechanism is only possible by considering the Umklapp process, and accounts for electron-electron relaxation when the laser electric field is zero.

2. Collision operators

The electron collision operators corresponds to the transition rate from a state $\mathbf{k}$ to a state $\mathbf{k}'$ [26,27]. Their amplitude is proportional to a matrix element, which depends on the nature of colliding particles. In order to evaluate the various matrix elements, the standard procedure considering a single electron Hamiltonian is used. Since the $e-pt-ph$ and $e-pt-e$ processes includes the $e-ph$ and $e-e$ collisions (as shown below the formalism including the laser electric field still stands when the latter vanishes), the Hamiltonian describing a single-electron oscillating in the laser electric field is considered. The total Hamiltonian reads in SI units

$$\widehat{H} = \frac{(\widehat{\mathbf{P}} - e\mathbf{A})^2}{2m_e} + V_{e-\text{lattice}}(\mathbf{r}) + V_{e-e}(\widehat{\mathbf{R}}) \quad (2)$$

where $\widehat{\mathbf{P}}$ is the momentum operator, e is the electron charge, m_e the electron mass, and $\mathbf{A}$ is the vector potential. $V_{e-\text{lattice}}$ and V_{e-e} are the interaction potentials with the lattice and other electrons, respectively. The interaction potential of an electron with the lattice reads $V_{e-\text{lattice}}(\mathbf{r}) = V^0_{e_i}(\widehat{\mathbf{r}}) + V_{e-ph}(\widehat{\mathbf{r}})$ where $V^0_{e_i}$ is the interaction potential of an electron with ions of the lattice in their equilibrium position, and V_{e-ph} the interaction with phonons [23]. The matrix elements are evaluated by using the picture of laser-assisted electron collisions, i.e., the interaction Hamiltonian is used with laser dressed wavefunctions [25,28–32],

$$\psi_m(\mathbf{k}, t) = u(\mathbf{k}) e^{i\mathbf{k}\cdot\mathbf{r} - \frac{i}{\hbar}\int_{-\infty}^{t} dt'(p^2 + e^2A^2(t') - 2e\mathbf{p}\cdot\mathbf{A}(t'))^2/2m_e} \quad (3)$$

where $u(\mathbf{k})$ is the unperturbed Bloch term of the wavefunction. $\mathbf{p}$ is the eigenvalue of the momentum operator $\widehat{\mathbf{P}} = -i\hbar\nabla$. Since femtosecond laser pulses are considered, including at least several optical cycles, the slowly varying envelope approximation is used, i.e., $A(t) = A_0(t)\cos(\omega t)$ where $A_0(t)$ is the envelope, then simplifying the temporal integration of transition amplitudes.

Regarding the $e-pt-ph$ collision, the general expression of the collision operator, accounting for both normal and Umklapp processes, then reads [18,25]

$$\begin{aligned}\left.\frac{\partial f(\mathbf{k})}{\partial t}\right|_{e-pt-ph} = \frac{1}{4\pi^2\hbar}\sum_{l,\pm,L,T}\int d\mathbf{k}' J_l^2\left(\frac{e\Delta\mathbf{p}\cdot\mathbf{F}}{m_e\hbar\omega^2}\right) \times \Bigg[&(1-f(\mathbf{k}))f(\mathbf{k}')\left(\frac{1\pm1}{2} + n(\pm\mathbf{k}' \mp \mathbf{k})\right)\left|\mathcal{M}^{L,T}_{\mathbf{k},\mathbf{k}'}\right|^2 \\ &\times \delta\left(E_{\mathbf{k}} \pm E^{L,T}_{ph}(\pm\mathbf{k}' \mp \mathbf{k}) - E_{\mathbf{k}'} + l\hbar\omega\right) - f(\mathbf{k})(1+f(\mathbf{k}'))\left(\frac{1\pm1}{2} + n(\mp\mathbf{k}' \pm \mathbf{k})\right)\left|\mathcal{M}^{L,T}_{\mathbf{k},\mathbf{k}'}\right|^2 \\ &\times \delta\left(E_{\mathbf{k}} \mp E^{L,T}_{ph}(\mp\mathbf{k}' \pm \mathbf{k}) - E_{\mathbf{k}'} + l\hbar\omega\right)\Bigg] \end{aligned} \quad (4)$$

where $E_{\mathbf{k}}$ stands for the electron kinetic energy in state $\mathbf{k}$. J_l is the Bessel function of order l, where the index l stands for absorption or emission of $|l|$ photons. Note that without external electric field $\mathbf{F}$ ($F = 0$), all terms J_l with $l \neq 0$ vanish and $J_0 = 1$, leading to the electron-phonon collision operator (only relaxation). The $\pm$ sum stands for emission and absorption of phonon, and $\Delta\mathbf{p}$ is the exchanged momentum during the collision i.e., $\Delta\mathbf{p} = \mathbf{p}(\mathbf{k}') - \mathbf{p}(\mathbf{k})$. $|M^{L,T}_{\mathbf{k},\mathbf{k}'}|^2 = |\langle\mathbf{k}'|V^{L,T}_{e-ph}(\mathbf{k}'-\mathbf{k})|\mathbf{k}\rangle|^2$ is the matrix element for the electron-phonon (longitudinal or transverse) coupling. E_{ph} is the phonon energy. n^L and n^T stand for distribution functions of longitudinal and transverse acoustic phonons [also denoted $n(q)$], respectively. Both are assumed to be equilibrium Bose-Einstein distributions at room temperature since their evolution is negligible on a femtosecond timescale [33]. The collision rate depends on the kind (longitudinal or transverse) of phonon as shown below.

Following a similar procedure, the collision operator for electron-electron interaction within the laser electric field reads [18,25]

$$\begin{aligned}\left.\frac{\partial f(\mathbf{k})}{\partial t}\right|_{e-pt-e} = \frac{2\pi}{\hbar}\frac{1}{(8\pi^3)^3}\sum_{l,\uparrow\uparrow,\uparrow\downarrow}\int d\mathbf{k}_1 d\mathbf{k}_2\, J_l^2\left(\frac{e\Delta\mathbf{p}\cdot\mathbf{F}}{m_e\hbar\omega^2}\right)\delta\left(E_{\mathbf{k}} + E_{\mathbf{k}_2} - E_{\mathbf{k}_1} - E_{\mathbf{k}_3} + l\hbar\omega\right) \\ \times\Big[(1-f(\mathbf{k}))(1-f(\mathbf{k}_1))f(\mathbf{k}_2)f(\mathbf{k}_3)|\mathcal{G}^{\uparrow\uparrow,\uparrow\downarrow}_{\mathbf{k},\mathbf{k}_2,\mathbf{k}_1,\mathbf{k}_3}|^2 \\ - f(\mathbf{k})f(\mathbf{k}_1)(1-f(\mathbf{k}_2))(1-f(\mathbf{k}_3))|\mathcal{G}^{\uparrow\uparrow,\uparrow\downarrow}_{\mathbf{k}_1,\mathbf{k}_3,\mathbf{k},\mathbf{k}_2}|^2\Big]_{\mathbf{k}_3=\mathbf{k}+\mathbf{k}_2-\mathbf{k}_1}, \end{aligned} \quad (5)$$

where $\Delta\mathbf{p}$ is total variation of momentum of the two-electron system, i.e., in the case where the initial state is $|\mathbf{k},\ \mathbf{k}_1\rangle$ and the final state is $|\mathbf{k}_2, \mathbf{k}_3\rangle$, $\Delta\mathbf{p} = \mathbf{p}(\mathbf{k}_3) + \mathbf{p}(\mathbf{k}_2) - \mathbf{p}(\mathbf{k}) - \mathbf{p}(\mathbf{k}_1)$. Note that in the case of free electrons with a parabolic band, since $\mathbf{p} = \hbar\mathbf{k}$ and $\Delta\mathbf{k} = \mathbf{0}$, $\Delta\mathbf{p} = 0$. Thus, since $J_{l\neq 0} = 0$ and $J_0 = 1$, the external electric field has no influence on this electron collision operator. Photon absorption is thus only possible through Umklapp processes for which $\Delta\mathbf{p} \neq 0$. $|\mathcal{G}^{\uparrow\uparrow,\uparrow\downarrow}_{\mathbf{k}_1,\mathbf{k}_3,\mathbf{k},\mathbf{k}_2}|^2$ stands for the electron-electron collision operator for parallel spins ($\uparrow\uparrow$) or antiparallel spins collisions ($\uparrow\downarrow$) [34].

The two collision operators [Eqs. (4) and (5)] account for all main processes leading to intraband transitions of conduction electrons. They are based on integrations over the vectorial wave-vector space. Such calculations are computationally expansive. The goal of the present paper is to provide an unified description of the out-of-equilibrium femtosecond electron dynamics accounting for experimental values of absorption, thermal conductivity, and electron-phonon coupling coefficient, for possible future studies; and highlight the role of Umklapp processes within this scope (by switching on or off each process). Therefore, the following approximations commonly made in the literature are used to simplify the theoretical description of the present physical system. (i) Since macroscopic quantities (optical absorption, thermal conductivity, and electron-phonon coupling coefficient) will be evaluated, the averaged collision frequencies of electrons with respect to the angle of $\mathbf{k}$ are considered. Thus, a mean isotropic dispersion relation, $E_\mathbf{k} = \hbar^2\mathbf{k}^2/2m_e$, in BZ1 is considered. Such an approximation is known to provide accurate value of free electron specific heat and Fermi velocity [23]. (ii) Laser-induced small perturbations of the distribution function are assumed (laser intensity is low enough). The collision frequencies may thus be assumed not to depend on the anisotropy of the perturbation, which could be induced directly by anisotropic photon absorption processes. Consistently with the approximation of isotropic dispersion relations, we then assume that $f(\mathbf{k}) = f(k)$, with $k = \|\mathbf{k}\|$. (iii) Because of the narrow photo-induced perturbation ($\hbar\omega < E_F$) of the energy distribution function, we assume that the exchanged energy during an electron-electron collision is small, so that according to the results of [34], collisions between electrons with parallel spin can be neglected due to the exchange term. Consistently, we assume that the matrix elements can be calculated within the approximation of the static screening due to valence and conduction electrons. The Thomas-Fermi formalism will then be used. (iv) For the phonons, we use the sine dispersion relation for both longitudinal and transverse phonons: $E^{L,T}_{ph}(\mathbf{k}) = \hbar v_{sL,T}\ \sin(\pi k/K)K/\pi$, where $E^{L,T}_{ph}(\mathbf{k})$ is the energy of phonon, and v_s is the sound speed. According to [35], $v_{sL} = 3240$ m/s and $v_{sT} = 1200$ m/s in gold. One should notice that there is one longitudinal and two transverse branches. We assume that the two transverse branches are degenerated. Such description gives good values for the maximum energy of the phonons [23].

As shown in forthcoming sections, these assumptions allows one in particular to obtain simplified matrix elements. For the sake of clarity, the collision operators can be split into three parts since each process is independent from each other,

$$\left.\frac{\partial f(\mathbf{k})}{\partial t}\right|_{e-pt-ep} = \left.\frac{\partial f(\mathbf{k})}{\partial t}\right|^{N}_{e-pt-ep} + \left.\frac{\partial f(\mathbf{k})}{\partial t}\right|^{U_1}_{e-pt-ep} + \left.\frac{\partial f(\mathbf{k})}{\partial t}\right|^{U_2}_{e-pt-ph} \tag{6}$$

where ep denotes an electron or a phonon. These collision operators are evaluated in Appendix A, Sec. II B, and Sec. II C, respectively.

TABLE I. Characteristic wave vectors involved in collisions for gold.

Wave vector	$K/2$ reciprocal lattice	k_F Fermi	q_0 screening
Values (10^{10} m^{-1})	1.5	1.2	0.9

B. U_1 process: Electron scattering out of the first Brillouin zone

1. Electron-photon-phonon collision

The importance of electron scattering out of BZ1 is demonstrated by analyzing the matrix element (A6), which quantifies the coupling between two electron states induced by a phonon. This matrix element filters the spatial component of the lattice potential larger than q_0. The typical crystalline momentum exchanged during an electron phonon collision is q_0; such transition being negligible if $q_0 \ll K$. Table I summarizes the values of the three main wave vectors, which matter for such collisions. One should notice that neglecting the energy of a phonon, the minimum value of Δk, for a transition from state k_F of BZ1 to state $K - k_F$ of BZ2, is $K - 2k_F = 0.6\ 10^{10}$ m$^{-1} < q_0$. This shows that U_1 processes should be considered.

The contribution of U_1 process is more complicated to evaluate compared with the N process due to two reasons: (i) First, in the delta function accounting for the energy conservation in Eq. (4); one should notice that (assuming parabolic band in BZ1) $E(\mathbf{k}' \in \text{BZ2}) = E(\mathbf{k}' - \mathbf{K}) = \hbar^2(\mathbf{k}' - \mathbf{K})^2/2m_e$ with $\mathbf{k}' - \mathbf{K} \in BZ_1$. Then, the angular dependence in the integration is not only due to the angle between $\mathbf{k}$ and $\mathbf{k}'$, but also due to the angle between $\mathbf{k}'$ and $\mathbf{K}$, which makes the integration over angles more complicated. Analytic simplifications, which enables to obtain electron-phonon collision operators for the N process cannot be achieved for the U_1 process. (ii) Secondly, since $\mathbf{k}$ and $\mathbf{k}'$ are not in the same Brillouin zone, the approximation of free electrons is no longer appropriate and one cannot assume in Eq. (A5) that $\int d\mathbf{r} u_\mathbf{k}(\mathbf{r}) u^\dagger_{\mathbf{k}'}(\mathbf{r}) = 1$, leading to Eq. (A6). As explained in the Sec. I, within the framework of developing an unified modeling of the femtosecond laser-induced electron dynamics while keeping a computationally efficient approach, in order to provide a tool allowing one to capture the main physical processes at play and understand the role of each process, here we propose a simplified description of Umklapp processes for the purpose of evaluation of macroscopic observables. The Fermi liquid theory considers Umklapp and N processes similarly. Since a

narrow electron energy range is considered, i.e., $|E - E_F| \leqslant \hbar\omega$, the U_1 e-pt-ph collision operator are thus considered to be proportional to the N one, with a proportionality coefficient $\alpha_{e-ph\ U_1}$. The only considered difference is in the argument of the Bessel function accounting for momentum conservation, $\Delta\mathbf{p} = \mathbf{p}(\mathbf{k}') - \mathbf{p}(\mathbf{k}) = \hbar(\mathbf{k}' - \mathbf{K} - \mathbf{k}) = \hbar(\mathbf{q} - \mathbf{K})$. The operator for the U_1 e-pt-ph process thus reads

$$\left.\frac{\partial f(\mathbf{k})}{\partial t}\right|_{e-pt-ph}^{U_1} = \frac{1}{2\pi\hbar^3}\frac{m_e}{k}\alpha_{e-ph\ U_1}\sum_{l,\pm} \times \int_0^{K/2} dqq\left|\mathcal{M}_q^L\right|^2 \overline{J_l^2}\left(\frac{e\sqrt{(q^2+K^2)}F}{m_e\omega^2}\right) \times \Big((1-f(k))\,f(k')\left(\frac{1}{2}\pm\frac{1}{2}+n(q)\right) - f(k)\,(1-f(k'))\left(\frac{1}{2}\mp\frac{1}{2}+n(q)\right)\Big)\Xi_\pm \tag{7}$$

where $|\mathcal{M}_q^L|^2$ is provided by Eq. (A6). $\Xi_\pm = 1$ if $((\frac{\hbar q}{2m_e} \pm \frac{E_{ph}}{\hbar q}) + l\frac{\omega_l}{q}) < \frac{\hbar k}{m_e}$, and $\Xi_\pm = 0$ other while. This approach thus includes a single adjustable parameter $\alpha_{e-ph\ U_1}$, which is set in Sec. III from a comparison to the measured imaginary part of the dielectric function. This process provides a further contribution to the optical absorption.

2. *Electron-photon-electron collision*

Electron-electron Umklapp processes are related to exchange crystalline momentum of the same order of magnitude as k_F [34], and thus should be introduced in the whole description of the electron dynamics. Similarly as for electron-phonon collisions (i.e., considering a narrow band of the spectrum of electrons, i.e., $|E - E_F| \leqslant \hbar\omega$), we assume that the main influence of the Umklapp process can be captured assuming there amplitude is proportional to the normal process. The only difference also appears in the conservation of energy, which has to account for photon absorption, and in the Bessel function argument where $\Delta\mathbf{p} \neq \hbar\Delta\mathbf{k}$. This electron-photon-electron Umklapp collision operator then reads

$$\left.\frac{\partial f(k)}{\partial t}\right|_{e-pt-e}^{U_1} = \frac{\pi\hbar}{32m_e}\frac{e^4}{\epsilon_0^2}\frac{1}{E_{TF}\sqrt{E}}\alpha_{e-e\ U_1}\sum_{l\neq 0}\int dE_2 dE_1 \frac{D(E_2+l\hbar\omega)}{k_2'}\frac{D(E_1)}{k_1}\left[\frac{\sqrt{\tilde{E}}}{(\tilde{E}+E_{TF})} + \frac{1}{\sqrt{E_{TF}}}\tan^{-1}\left(\sqrt{\tilde{E}/E_{TF}}\right)\right]_{\tilde{E}_{low}}^{\tilde{E}_{up}} \times \overline{J_l^2}\left(\frac{eKF}{m_e\omega^2}\right)([1-f(k)][1-f(k_1)]\times f(k(E_2+l\hbar\omega))f(k_3) + f(k)f(k_1)[1-f(k(E_2+l\hbar\omega))]\times[1-f(k_3)])|_{E_3=E+E_1-E_2-l\hbar\omega} \tag{8}$$

with $\tilde{E}_{up} = \min((\sqrt{E}+\sqrt{E_2+l\hbar\omega})^2; (\sqrt{E_1}+\sqrt{E_3})^2)$ and $\tilde{E}_{low} = \max((\sqrt{E}-\sqrt{E_2+l\hbar\omega})^2; (\sqrt{E_1}-\sqrt{E_3})^2)$. Note that the sum over l does not include the configuration $l = 0$, i.e., the e-e relaxation. The latter does not contribute significantly to the relaxation compared with the N process because the Umklapp process involves larger exchanged electron momentum and subsequently a smaller transition matrix element as shown by Eq. (A9). The $l = 0$ relaxation contribution has been removed within the above mentioned scope of developing a simplified approach allowing one to understand the main physical processes at play, and which is computationally efficient. The parameter $\alpha_{e-e\ U_1}$ is set in Sec. III.

C. U_2 process: Electron scattering by longitudinal and transverse phonons

Because of the periodicity of the lattice and due to its discrete nature, the electron-phonon potential does not only exhibits a component in $\mathbf{k} = \mathbf{q}$, but also in all the components $\mathbf{k} = \mathbf{q} + \mathbf{K}$. In this section, we present an approach to evaluate the contribution of this second kind of Umklapp process.

Considering Eq. (A3), three configurations may take place depending on the orientation of $\mathbf{e_q}$: (i) $\mathbf{e_q}$ is oriented along $\mathbf{q}$. In this configuration Eq. (A3) stands for electron-longitudinal-phonon coupling. (ii) $\mathbf{e_q}$ is orthogonal to the ($\mathbf{q}$, $\mathbf{K}$) plane, which leads to $V_{e-ph}(\mathbf{r}) = 0$. (iii) $\mathbf{e_q}$ is into the ($\mathbf{q}$, $\mathbf{K}$) plane and orthogonal to $\mathbf{q}$, leading to a non zero contribution to V_{e-ph} since $\mathbf{e_q}\cdot\mathbf{K} \neq 0$. Equation (A3) can also be written as

$$V_{e-ph}(\mathbf{r}) = \sum_{\mathbf{q},n} V_{e-ph}^n(\mathbf{q})e^{i\,\mathbf{q}\cdot\mathbf{r}} \tag{9}$$

where the index n denotes the transverse and longitudinal phonon bands. The longitudinal and transverse coupling are represented schematically in Fig. 1 considering respectively phonon with polarization vector $\mathbf{e}_{\mathbf{q}\parallel}$ and $\mathbf{e}_{\mathbf{q}\perp}$.

For the longitudinal N process, $\mathbf{K} = \mathbf{0}$ and $\mathbf{e_q}\cdot\mathbf{q} = q$ while for the transverse N process, $\mathbf{e_q}\cdot\mathbf{q} = 0$. Noting that for Umklapp processes, the angle between $\mathbf{e_q}$ and $\mathbf{K}$ can take any value, the longitudinal and transverse phonon-electron potential then reads

$$V_{e-ph}^{L,U_2}(\mathbf{q}) = \sum_{\mathbf{K}\neq\mathbf{0}} \delta R_{\mathbf{q}} V_{\mathbf{q}+\mathbf{K}}\left(q + \mathbf{e}_{\mathbf{q}}^L\cdot\mathbf{K}\right)e^{i\,\mathbf{K}\cdot\mathbf{r}}, \tag{10}$$

$$V_{e-ph}^{T,U_2}(\mathbf{q}) = \sum_{\mathbf{K}\neq\mathbf{0}} \delta R_{\mathbf{q}} V_{\mathbf{q}+\mathbf{K}}\mathbf{e}_{\mathbf{q}}^T\cdot\mathbf{K}\,e^{i\,\mathbf{K}\cdot\mathbf{r}}. \tag{11}$$

.

Equations (A5) and (A6) are two expressions for the electron-phonon matrix element. The first is obtained from the general expression (A3), which requires to have an analytic expression for $(\mathbf{q}+\mathbf{K})\cdot\delta\mathbf{R}_{\mathbf{q}}\,V_{\mathbf{q}}$. The second expression is analytic but only accounts for normal coupling between electrons and longitudinal phonons. By following the standard procedure of second quantization formalism [26,27], the matrix element within deformation potential theory for

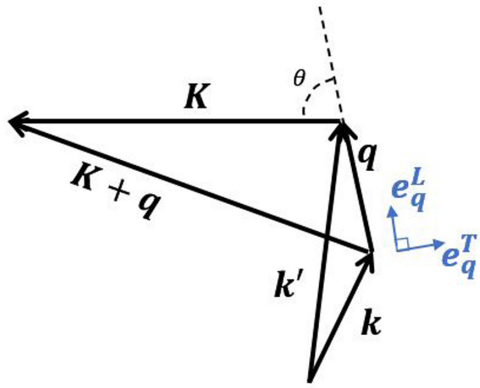

FIG. 1. Schematic representation of the diffusion of an electron by phonon Umklapp processes. An electron in the initial state $\mathbf{k}$ absorbs a phonon with crystalline momentum $\mathbf{q}$ and reach the state $\mathbf{k}' = \mathbf{k} + \mathbf{q}$. It is well known that such normal diffusion process is possible only if the phonon has a longitudinal polarization. However, phonons potential exhibits components in higher Brillouin zone than the first one. Thus, diffusion with transverse phonons may occurs and must be taken into account.

electron-phonon interaction (normal and Umklapp) has been obtained in semiconductors [10]. By identifying the dielectric deformation potential used in the matrix element to the matrix element pertaining to free electrons in metals [i.e., identifying general expression (A3) to expression (A6)], expression (A6) can be evaluated in the case where $\mathbf{K} \neq \mathbf{0}$,

$$\left|\mathcal{M}^L_{\mathbf{q},\mathbf{K}}\right|^2 = \frac{E^L_{ph}(q)e^2}{2\varepsilon_0\varepsilon_c^0\left(|\mathbf{q}+\mathbf{K}|^2+q_0^2\right)}\frac{\left(q+\mathbf{e}^L_{\mathbf{q}}\cdot\mathbf{K}\right)^2}{|\mathbf{K}+\mathbf{q}|^2}. \tag{12}$$

Note that according to the Bloch theorem, the final state of the electron is $\psi(\mathbf{k}+\mathbf{q}+\mathbf{K}) = \psi(\mathbf{k}+\mathbf{q})$. This will be taken into account for the collision operators and for photon absorption processes.

Similarly, considering Eqs. (A3) and (11), the transverse term reads

$$\left|\mathcal{M}^T_{\mathbf{q},\mathbf{K}}\right|^2 = \frac{E^T_{ph}(q)e^2}{2\varepsilon_0\varepsilon_c^0|\mathbf{q}+\mathbf{K}|^2+q_0^2}\frac{\left(\mathbf{e}^T_{\mathbf{q}}\cdot\mathbf{K}\right)^2}{|\mathbf{K}+\mathbf{q}|^2}. \tag{13}$$

As for longitudinal phonons, if $\mathbf{k}+\mathbf{q} \in BZ_1$, within the free electrons approximation in BZ1, $\Delta\mathbf{p} = \hbar\mathbf{q}$. Note that half of the transverse phonons have a polarization orthogonal to the $\mathbf{k}$, $\mathbf{K}$ plane while half have polarization into the plane. Thus the mean matrix element should by twice smaller, which leads to a factor 1/4 for $|\mathcal{M}^T_{\mathbf{q},\mathbf{K}}|^2$ instead of 1/2 for $|\mathcal{M}^L_{\mathbf{q},\mathbf{K}}|^2$. Thus, defining θ the angle between $\mathbf{q}$ and $\mathbf{K}$, the U_2 matrix elements read

$$\left|\mathcal{M}^L_{\mathbf{q},\mathbf{K}}\right|^2 = \frac{E^L_{ph}(q)e^2}{2\varepsilon_0\varepsilon_c^0\left(q^2+K^2+2Kq\cos\theta+q_0^2\right)}\frac{q^2+K^2\cos^2\theta+2Kq\cos\theta}{q^2+K^2+2Kq\cos\theta}, \tag{14}$$

$$\left|\mathcal{M}^T_{\mathbf{q},\mathbf{K}}\right|^2 = \frac{1}{4}\frac{E^T_{ph}(q)e^2}{\varepsilon_0\varepsilon_c^0\left(q^2+K^2+2Kq\cos\theta+q_0^2\right)}\frac{K^2\sin^2\theta}{q^2+K^2+2Kq\cos\theta}. \tag{15}$$

We now assume that the total collision operators can be obtained by considering mean angles, i.e., $\cos\theta \to \frac{1}{\pi}\int_0^\pi \cos\theta\sin\theta d\theta = 0$ and $\cos^2\theta \to \frac{1}{\pi}\int_0^\pi \cos^2\theta\sin\theta d\theta = 1/3$. Within this consideration, the matrix elements read

$$\left|\mathcal{M}^L_{\mathbf{q},\mathbf{K}}\right|^2 = \frac{E^L_{ph}(q)e^2}{2\varepsilon_0\varepsilon_c^0\left(q^2+K^2+q_0^2\right)}\frac{q^2+K^2/3}{q^2+K^2}, \tag{16}$$

$$\left|\mathcal{M}^T_{\mathbf{q},\mathbf{K}}\right|^2 = \frac{1}{6}\frac{E^T_{ph}(q)e^2}{\varepsilon_0\varepsilon_c^0\left(q^2+K^2+q_0^2\right)}\frac{K^2}{q^2+K^2}. \tag{17}$$

Note that with $K = 0$, Eq. (16) reduces to Eq. (A6), the matrix element for the N process, while Eq. (17) reduces to zero.

III. RESULTS AND DISCUSSION

The previously presented developments aiming at accounting for the absorption, the thermal conduction coefficient, and the electron-phonon coupling coefficient, include two adjustable parameters, $\alpha_{e-pt-ph\,U_1}$ and $\alpha_{e-e\,U_1}$. Our method to predict these three physical quantities consists of first setting the value of $\alpha_{e-pt-ph\,U_1}$ and $\alpha_{e-e\,U_1}$ to account for the measured imaginary part of the dielectric function. Then, without further procedure, both the thermal conductivity and electron-phonon coupling coefficient are evaluated (obtained values of $\alpha_{e-pt-ph\,U_1}$ and $\alpha_{e-e\,U_1}$ are not changed). Such an approach also allows us to evaluate the contributions of various processes.

A. Influence of Umklapp processes on photon absorption

To evaluate $\alpha_{e-pt-ph\,U_1}$ and $\alpha_{e-e\,U_1}$, the experimental value of the imaginary part of the dielectric function $\mathrm{Im}(\varepsilon)$ in the intraband domain is considered. The experimental data of [36] are chosen as a reference due to their relatively recent publication and critical comparison to previously published results in the literature. $\mathrm{Im}(\varepsilon)$ can be theoretically evaluated from the kinetic approach by considering the variations in the density of energy of the electron gas, $\langle E\rangle$, induced by the external laser electric field [9,25],

$$\frac{\partial\langle E\rangle}{\partial t} = \frac{\omega\varepsilon_0\mathrm{Im}(\varepsilon)}{2}F^2, \tag{18}$$

where F is the laser electric field amplitude. The variations in the density of energy also reads in terms of collision operators

$$\frac{\partial\langle E\rangle}{\partial t} = \int D(E)E\left(\left.\frac{\partial f}{\partial t}\right|_{e-pt-ph} + \left.\frac{\partial f}{\partial t}\right|_{e-pt-e}\right)dE \tag{19}$$

where the contribution of pure (without laser electric field) relaxation processes is not included. Then, Eqs. (18), (19), and previous modeling of collision operators allow us to calculate $\mathrm{Im}(\varepsilon)$. Collision operators and $\mathrm{Im}(\varepsilon)$ are calculated numer-

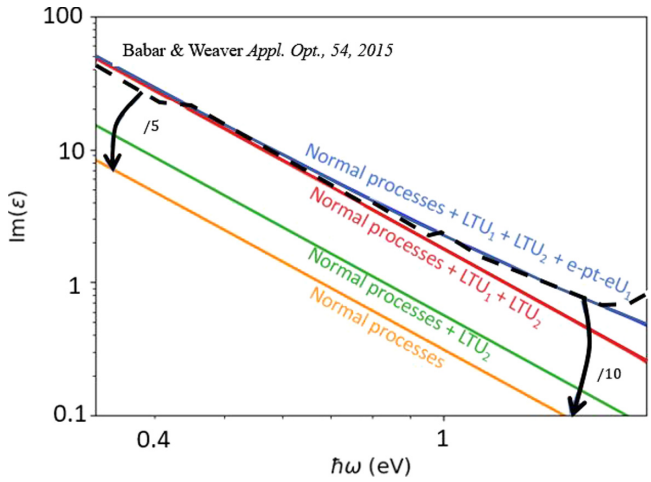

FIG. 2. Imaginary part of the intraband permittivity as a function of the photon energy. The dashed-black curve corresponds to experimental data of Babar and Weaver [36]. The other curves are obtained with the present modeling where various processes are step-by-step considered [Eqs. (18) and (19)]. The orange curve is obtained with N processes only. The green curve further includes the U_2 process. In addition to previous processes, the U_1 e-pt-ph is included to obtain the red curve. The whole modeling is used for the blue curve.

ically with a discretization of electron distribution functions with a 1-meV-energy step. The convergence has been verified.

Figure 2 shows the evolution of the imaginary part of the dielectric function with respect to the photon energy as theoretically predicted by our approach and as experimentally obtained by Babar and Weaver [36]. The contributions of various absorption mechanisms are depicted. Only considering the electron transitions in BZ1, Im(ε) is underestimated by a factor of 5 and 10 in the low and high photon energy domain, respectively. As shown in the Appendix B, Im(ε) scales as ω^{-3}, which corresponds to experimental observations at low photon energies. This region corresponds to a classical interaction regime, which is correctly described by the Drude model for $\omega \gg \nu$ where ν stands for the total electron collision frequency. By additionally accounting for the U_2 processes (green curve), Im(ε) is increased by a factor of 2 and still behaves as ω^{-3}. Indeed, the explanation, which has been provided for N processes is still appropriate for these processes and Im(ε) still follows the same scaling law as classical Drude prediction with constant collision frequency. The predicted value of Im(ε) still remain significantly lower than experimental data.

The Drude model including a constant collision frequency or only the e-ph collision frequency fails to describe Im(ε) at optical frequencies because of the deviation from the ω^{-3} scaling law of Umklapp electron-photon-electron processes [37]. Absorption induced by this process is expected to be negligible at low $\hbar\omega$, and of the same order of magnitude as $e-pt-ph$ processes at optical frequencies [38]. Such a behavior allows us to set the value of $\alpha_{e-pt-ph\ U_1}$ and $\alpha_{e-e\ U_1}$ independently. $\alpha_{e-pt-ph\ U_1}$ has been set to fit the measured imaginary part of the dielectric function [36] at low photon energies ($\hbar\omega \leqslant 0.6$ eV). $\alpha_{e-e\ U_1}$ has then been set to fit the measured imaginary part of the dielectric function on the whole spectrum. A very good agreement with experimental observations is obtained with $\alpha_{e-pt-ph\ U_1} = 0.2$ and $\alpha_{e-e\ U_1} = 0.75$ as shown in Fig. 2.

Despite the relatively low contribution of 20% of the U_1 process to the pure electron scattering (relaxation), the absorption is increased by a factor of 3. Such a different contribution can be explained comparing $N+U_2$ and $N+U_1+U_2$ $e-pt-ph$ collision frequencies. According to Eq. (32), the N $e-pt-ph$ absorption process scales with $\overline{J_l^2}(\frac{e\hbar qF}{m_e\hbar\omega^2})$ while U_1 processes scale as $\alpha_{e-ph\ U_1}\overline{J_l^2}(\frac{e\hbar\sqrt{q^2+K^2}F}{m_e\hbar\omega^2})$. For a small enough laser electric field (where absorption is mainly linear), i.e., $\frac{eKF}{m_e\omega^2} \ll 1$, only the contribution of $l=1$ should be kept, which leads to $\overline{J_l^2}(\frac{eKF}{m_e\omega^2}) = \delta_{l,0} + \delta_{l,1}\overline{(\frac{eK\mathcal{E}}{2m_e\omega^2})^2}$ [25] where $\delta_{ll'}$ stands for the Kronecker symbol: $\delta_{ll'}=1$ if $l=l'$ and 0 otherwise. The ratio of $(N+U_1+U_2)$ contribution processes over the $(N+U_2)$ one reads $1+\alpha_{e-pt-ph\ U_1}(1+\frac{K^2}{q^2})$. Considering that typically $q \sim q_0$ and using the parameters summarized in Table I, the $e-pt-ph$ collisions including $N+U_1+U_2$ processes are roughly 3 times more efficient than those only including $N+U_2$ processes. This further demonstrates the importance of the distinction between the eigenvalue of the momentum operator (which is essential to understand photon absorption), and the crystalline momentum.

Regarding $\alpha_{e-e\ U_1}$, its value larger than the one of $\alpha_{e-pt-ph\ U_1}$ can be explained with two arguments: (i) $e-e$ Umklapp processes are due to a small part of $\uparrow\downarrow$ and a significant part of $\uparrow\uparrow$, which are assumed to be negligible for N processes. Such consideration of $\uparrow\uparrow$ or $\uparrow\downarrow$ are not relevant for $e-ph$ collision processes. (ii) One should also consider the case where two electrons reaches BZ2. In such a configuration the variation of total momentum can be higher than $\hbar\mathbf{K}$ and the mean absorbed power should be much higher. This argument is not relevant for $e-pt-ph$ processes since only one single electron is involved in the process. The fit of the parameters implicitly account for this phenomenon.

B. Influence of Umklapp processes on collision frequencies and electron-phonon coupling constant

By writing the collision operator as

$$\left.\frac{\partial f(\mathbf{k})}{\partial t}\right|_{\text{coll}} = (1-f(\mathbf{k}))\,S^{+}(\mathbf{k}) - f(\mathbf{k})S^{-}(\mathbf{k}) \qquad (20)$$

one obtains the standard Drude-Sommerfeld electric conductivity $\sigma = n_e v_F^2/3\nu_{e-ph}$ and associated thermal conductivity $\kappa_e = C_e v_F^2/3\nu_{e-ph}$ [39] with an effective electron-phonon collision frequency $\nu_{e-ph} \approx S^{+}_{e-ph}(k_F) + S^{-}_{e-ph}(k_F)$ when $T_e \ll E_F$ [9,23]. In our calculations, $S^{+}(\mathbf{k})$ and $S^{-}(\mathbf{k})$ are obtained by identifying Eq. (20) to Eq. (4) with respect to $(1-f(\mathbf{k}))$ and $f(\mathbf{k})$, respectively.. At 300 K, κ_e is of the order of 300 W m^{-1} K^{-1} with values slightly evolving depending on the published studies [39–42].

Figure 3 shows the evolution of this effective electron-phonon collision frequency as a function of the electron energy at $T_e = T_{ph} = 300$ K. The contribution of various processes (N, U_1, or U_2) is highlighted. When only N processes are considered, $S^{+}(E_F) + S^{-}(E_F) \approx 20$ ps^{-1} at the Fermi level, which leads to a static electric and thermal

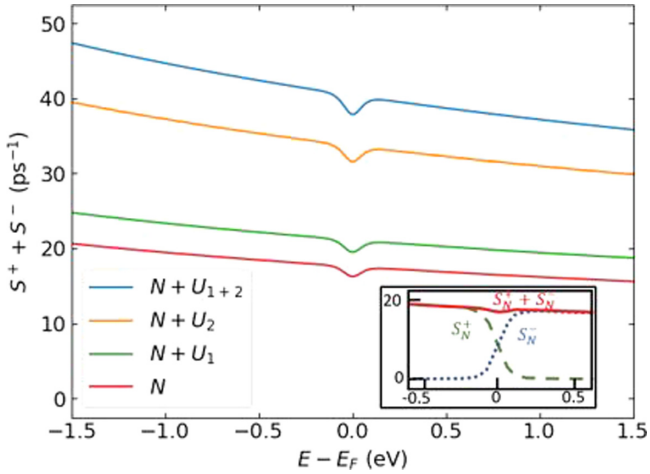

FIG. 3. Total electron-phonon collision frequencies with respect to electron energy accounting for N processes only (red line), $N + U_1$ processes (green line), $N + U_2$ processes (orange line), $N + U_1 + U_2$ processes (blue line). These collision frequencies have been calculated with $\mathbf{F} = \mathbf{0}$ in Eq. (4). The inset shows the separate contribution of S^+ and S^- for normal processes (units are the same as the main graph).

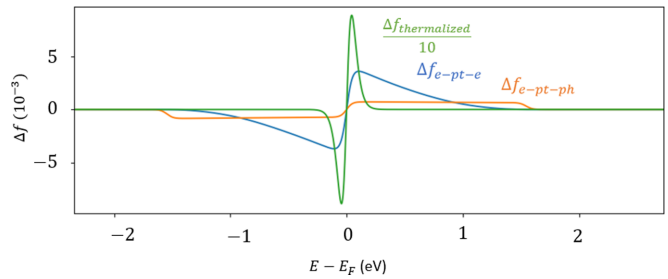

FIG. 4. Perturbations of electron distribution function with a same total absorbed energy (associated to an increase of electron temperature about 40 K) induced by an increase of the electron temperature (green line), electron-photon-phonon processes (orange line), and electron-photon-electron Umklapp processes (blue line). Note that these perturbations are obtained just after the excitation process, without any relaxation process.

conductivities twice larger than the experimental one (corresponding to a collision frequency of $\sim$40 ps^{-1} [23]). When the contribution of Umklapp processes is considered, $S^+(E_F) + S^-(E_F) = 40$ ps^{-1}, which is in a very good agreement with standard electron-phonon collision frequencies and associated electrical conductivity [23]. Regarding the thermal conductivity, with $v_F = 1.39 \times 10^6$ m/s and $C_e = 1.9 \times 10^4$ J m^{-3} K^{-1} [39], we obtain $\kappa_e \sim 306$ W m^{-1} K^{-1}, which is in a good agreement with values provided in the literature. The U_1 process increases the electron-phonon collision frequencies by 20%, which is consistent with the fact that the contribution of the U_1 processes is proportional to Normal processes with a coefficient $\alpha_{e-ph\ U_1} = 0.2$ (as set in the previous section to account for absorption properties of gold). The U_2 process increases electron-phonon collision frequencies by 50%, while it is 100% for photon absorption. Indeed, the phase space, which can be reached during an $e - ph$ collision is mainly limited by the maximum energy of a phonon while it is limited by the energy of a photon for photon absorption (at optical frequencies, phonon energy is negligible with respect to photon energy). Thus, the contribution of transverse phonons, which have similar crystalline momentum but lower energy than longitudinal phonons, is lower for $e - ph$ processes than for $e - ph - pt$ one.

Note that the collision frequency exhibits a decrease with respect to the electron energy with a local minimum at the Fermi energy. This behavior can be explained with the Fermi liquid theory: for $E - E_F > k_B T_e + k_B \theta_D$, an electron, which generates a phonon cannot loss more energy than $k_B \theta_D$, where θ_D is the Debye temperature. Thus, the energy of the final state is larger than $E_F + k_B T_e$ where states are completely empty. The Pauli exclusion principle has no influence on the collision frequency. On the other hand, for $E - E_F \approx k_B T_e + k_B \theta_D$, the final state is partially occupied due to thermal smoothness of the distribution function. When $E - E_F < -k_B T_e$ the final electron state due to the emission of a phonon is necessary fully filled, and $S^- = 0$. Thus the electron-phonon collision frequency S^- increases from zero to its maximum value between $E_F - k_B T_e$ and $E_F + k_B(T_e + \theta_D)$. Similarly, S^+ decreases to zero between $E - E_F = -k_B(T_e + \theta_D)$ to $E - E_F \approx k_B T_e$. Finally, $S^+ + S^-$ exhibits a local minimum at $|E - E_F| \lesssim k_B(T_e + \theta_D)$. This analysis is supported by the inset in Fig. 3.

Within the present formalism, the electron-phonon coupling constant G of the two-temperature model can also be evaluated owing to the following relation:

$$\frac{\partial \langle E \rangle}{\partial t} = \int E \left. \frac{\partial f}{\partial t} \right|_{e-ph} dE = G\,(T_l - T_e), \qquad (21)$$

where T_l and T_e denote the initial lattice and electron temperatures used to define phonon and electron distribution functions (Bose-Einstein and Fermi-Dirac, respectively). Setting $T_{ph} =$ 300 K and $T_e = 350$ K, which accounts for conditions of [5,24] for instance, numerical simulations lead to $G = 3 \times 10^{16}$ W/m^3/K. This result is in good agreement with [9]. Note that this result is found not to depend on the electron temperature as long as $T_{ph} < \theta_D$ and $T_e \ll E_F$ as predicted in [8]. We have checked that the same value of G is obtained with various values of T_e in a similar range.

C. Influence of the e-pt-e process on the electron energy distribution

The $e - pt - e$ process has been shown to contribute significantly to the absorption for large enough photon energies, i.e., it contributes significantly to the electron dynamics. However, models that do not include this collisional process are able to account for some experimental observations [5,24]. The aim of the present section is to elucidate this contradictory observations. For this purpose, the influence of the $e - pt - e$ process on the shape of the electron energy distribution is first investigated. The perturbation of the distribution function Δf for a same total absorbed energy $\langle \Delta E \rangle$ induced by $e - pt - ph$ and $e - pt - e$ processes is shown in Fig. 4. The $e - pt - ph$ perturbation exhibits the well known two-step distribution on the energy range from $E_F - \hbar\omega$ to $E_F + \hbar\omega$ [18,24,33] accounting for the fact that the electron energy

variation cannot be larger than the photon energy. This shape of the distribution is due to the fact that the photon absorption probability assisted by a phonon is mainly driven by the initial step-like Fermi-Dirac distribution [for $k_B T_e$ (andθ_D) $\ll \hbar\omega \ll E_F$], leading to a relatively constant excitation probability regardless the final electron energy. The mean energy of excited electrons is thus $\overline{E}_{e-pt-ph} = \frac{\int_{E_F}^{\infty} dE\ D(E) E \Delta f_{e-pt-ph}}{\int_{E_F}^{\infty} dE\ D(E) \Delta f_{e-pt-ph}} \approx \hbar\omega/2$.

Regarding the $e-pt-e$ process, the mean energy of carriers $\int_{E_F}^{\infty} \Delta f D(E) E dE$ is $\hbar\omega/4$ as already pointed out with qualitative arguments [38]. Indeed, the pair of excited electrons, originating from the energy interval $[E_F - \hbar\omega; E_f]$ due to the initial energy distribution, makes a transition towards the energy range $[E_F; E_F + \hbar\omega]$ due to the absorption of one photon. The mean energy of the pair of electrons is thus $\hbar\omega/2$, and the mean energy of a single electron then is $\hbar\omega/4$. An explanation of the shape of the energy distribution perturbation can also be provided by considering the initial step-like shape electron energy distribution. Considering two electrons indexed 1 and 2, the energy conservation involves $E_1^f + E_2^f = E_1^i + E_2^i + \hbar\omega$ where superscripts i and f denote the initial and final states, respectively. Due to the initial Fermi-Dirac distribution, a transition is possible if E_1^i and E_2^i are between $E_F - \hbar\omega$ and E_F. More precisely, since the final energy of both electrons must be larger than E_F, if $E_1^i = E_F - \alpha\hbar\omega$, with α a parameter in between 0 and 1, imposes $E_2^i > E_F - (1-\alpha)\hbar\omega$. Therefore, the larger α (or smaller E_1^i), the smaller the number of configurations for electron 2 satisfying transition rules. For instance in the limit cases, electron 1 with energy $E_1^i = E_F - \hbar\omega$ ($\alpha = 1$) can collide with electron 2 at energy $E_2^i = E_F$; and electron 1 with energy $E_1^i = E_F$ ($\alpha = 0$) can only collide with electron 2 with energies E_2^i in between E_F and $E_F - \hbar\omega$. Assuming a constant density of states (because $\hbar\omega \ll E_F$), the $e-pt-e$ collision probability is proportional to the above mentioned number of configurations, explaining the rather linear evolution of Δf on the intervall $[E_F - \hbar\omega; E_f]$. The symmetric shape on the energy intervall $[E_F; E_f + \hbar\omega]$ is explained with the same arguments.

For $e-pt-ph$, since the photon energy is absorbed by one single electron while it must be shared between two electrons for $e-pt-e$ collision, $\overline{E}_{e-pt-ph} \approx 2\overline{E}_{e-pt-e}$. This also explains why $\max(\Delta f_{e-pt-e}) \approx 4\ \max(\Delta f_{e-pt-ph})$. The total energy $\langle \Delta E \rangle$ associated to a distribution of carriers reads: $\langle \Delta E \rangle \approx \overline{E} \Delta n_e$, where Δn_e stands for the number of carriers, $\Delta n_e \approx 2\, D(E_F) \overline{E} \Delta f$. That leads to $\Delta f \propto \frac{\langle E \rangle}{D(E_F)\, \overline{E}^2}$.

Since phonon- and electron-assisted photon absorption processes lead to different electron energy distribution, their relaxation dynamics is also expected to be different because the electron relaxation time depends on the electron energy as $1/(E-E_F)^2$ (due to $e-e$ scattering). To exhibit the influence of a particular heating process on the dynamics of the distribution function, the temporal evolution of the electron energy distribution is investigated by considering either the $e-pt-ph$ process for the laser heating, or only the $e-pt-e$ mechanism. For that purpose, we have carried out numerical simulations based on the resolution of Boltzmann equation (1) where only the electron-electron scattering has been taken into consideration for the relaxation process. The

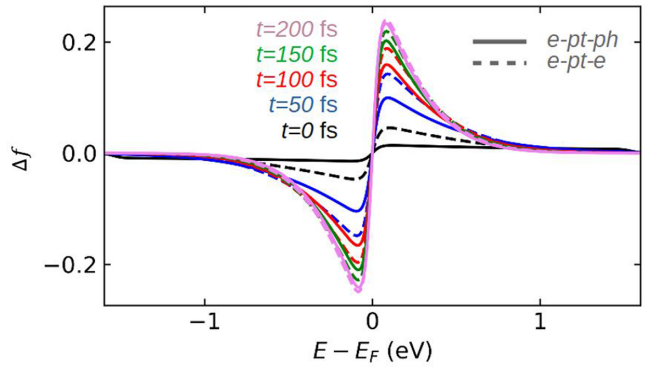

FIG. 5. Perturbations of the electronic distribution function for a same total absorbed energy (100 J/cm^3 deposited in 20 fs, see text) as predicted by the present modeling. Solid lines stand for the case where only $e-pt-ph$ processes have been considered for photon absorption while dashed lines stand for the case where only $e-pt-e$ processes have been considered for photon absorption. Only electron-electron relaxation processes has been considered [electron-phonon relaxation takes place on longer time scales ($t >$ 500 fs)]. Each color stands for a given simulation time.

laser pulse parameters are as follows. The laser intensity profile is $F^2(t) = F_0^2 \cos^2(\pi t/\Delta t_{FWHM})$ with $\Delta t_{FWHM} = 20$ fs (simulations start at $t = -\Delta t_{FWHM}/2$), and the photon energy is 1.5 eV. F_0 has been set to obtain the same total absorbed energy in both cases, i.e., 100 J/cm^3. The perturbation of the electron distribution at various time in both cases is plotted in Fig. 5 where the standard Euler method for time integration of Eq. (1) is used, with time and energy steps of 1 fs and 5 meV, respectively. At $t = 0$, the same results as Fig. 4 is obtained, accounting for the fact that electron relaxation is not yet efficient on this timescale. The maximum amplitude of the distribution perturbation induced by the $e-pt-e$ heating process is roughly four times larger than in the $e-pt-ph$ configuration. On a timescale of 100 fs, both distributions become rather similar, with a relative difference smaller than 10%. Thus, both distribution functions cannot been distinguished on timescales longer than 100 fs. The e-pt-e process thus contributes to absorption, but its influence on the shape of the electron energy distribution is negligible for timescales longer than 100 fs. This result explains why modeling not including the e-pt-e process is able to account for pump-probe experiments with a temporal resolution longer than 100 fs [5,24].

Within this model, we have also performed a full numerical resolution of Boltzmann equation in order check that our approach is able to reproduce the out-of-equilibrium electron distribution dynamics, which was shown in the literature to account for those experimental observables obtained with pump-probe experiments [5,24]. For timescales longer than 100 fs, a very good agreement with published theoretical results is obtained, further validating our approach.

IV. CONCLUSIONS

Earlier models proposed in the literature, based on solving the Boltzmann equation within the approximation of free electrons, describe partially the ultrafast electron dynamics

in gold induced by a femtosecond laser pulse. A correct description of transient optical properties of nano objects was achieved by evaluating accurately the electron-electron scattering and electron-phonon coupling coefficient. However, both electron-phonon collision frequency and optical absorption are underestimated, in particular the latter by one order of magnitude.

By including collisional Umklapp processes, we reproduce quantitatively all main experimental observables including the femtosecond laser induced electron dynamics, optical absorption, thermal conductivity, and electron-phonon coupling coefficient. Two kinds of Umklapp electron-phonon collision and one kind of Umklapp electron-electron interaction have been introduced. For the first kind of Umklapp electron-phonon collision, the electron is scattered into BZ2. The exchanged momentum can be much larger than the momentum of the phonon, increasing significantly the laser absorption (by a factor of 3) whereas the total electron-phonon collision frequency is modified by only ≈20% (thus weakly impacting the transport coefficient already accurately predicted by earlier models). The second kind of Umklapp electron-phonon collision is due to the periodicity of the discrete lattice, leading to an electron coupling with both longitudinal and transverse phonons. We have found that those processes account for half of the total electron-phonon and electron-photon-phonon collision frequencies.

Regarding electron-photon-electron collisions, they contribute to half of the total laser absorption for large enough photon energies. We have shown their significant influence on the scaling law of the imaginary part of the dielectric function (accounting for absorption) with respect to the photon energy, which is in a good agreement with experimental observations. The electron energy distributions induced by electron-photon-electron collisions and electron-photon-phonon collisions exhibit different shapes. By including the first process, the mean energy of electrons is twice smaller while the number of carriers is four times larger. However, due to electron-electron relaxation processes, both distributions become similar on a timescale longer than ∼100 fs. This result explains why earlier models neglecting the electron-photon-electron process are able to account for pump-probe experimental observations of the transient evolution of the electron energy distribution with a temporal resolution of the order of 100 fs. The signature of the electron-photon-electron collisions on the distribution shape is removed on this timescale.

The previous results have been obtained with a theoretical description including two adjustable parameters. They are sufficient to account for the values of the absorption with two different scaling with the photon energy, the thermal conductivity, and the electron-phonon coupling coefficient. That makes strong the fitting constrains, providing an evidence of the reliability of the present approach. The latter thus appears suitable for application purposes involving the ultrafast electron dynamics, e.g., the hot carrier photocatalysis, the modifications of the electron energy distribution at timescales shorter than 100 fs may play a significant role; they may impact the hot-carrier generation efficiency for instance. Pump-probe experiments with a 10-fs-temporal resolution are likely able to highlight the contribution of electron-photon-electron collisions.

APPENDIX A: *N* PROCESS: ELECTRON SCATTERING IN THE FIRST BRILLOUIN ZONE

Collision operators for N electron-phonon and electron-electron scattering can be found in [5,10,18,23,24,33]. They are recalled in the this section as they stand for the keystone for the development of Umklapp collision operators.

1. Electron-photon-phonon collision

The expression of the electron-phonon interaction potential is first recalled. Because of thermal motion, the ions of the lattice oscillate around their equilibrium position. Thus, the total electron-lattice interaction potential can be split into two terms through an expansion around the equilibrium position [10,18,23],

$$V_{e,\text{lattice}}(\mathbf{r}) = \sum_{\alpha} V_{e-i}\left(\mathbf{r} - \mathbf{R}_{\alpha}^{0}\right) - \delta\mathbf{R}_{\alpha}^{0} \cdot \nabla_{\mathbf{R}_{\alpha}^{0}} V_{e-i}\left(\mathbf{r} - \mathbf{R}_{\alpha}^{0}\right) \tag{A1}$$

where $\mathbf{r}$ denotes the position of the electron, $\mathbf{R}_{\alpha}^{0}$ the equilibrium position of the ion denoted by the index α, $\delta\mathbf{R}_{\alpha}^{0}$ the displacement of ion α, and V_{e-i} the electron-ion potential. The second term in Eq. (A1) is a perturbation accounting for the electron-phonon interaction. The matrix element associated with an electron transition induced by the electron-phonon potential involves a Fourier transform of the latter, which reads

$$V_{e-ph}(\mathbf{r}) = \sum_{\mathbf{q}} V_{e-ph}(\mathbf{q}) e^{i\,\mathbf{q}\cdot\mathbf{r}}. \tag{A2}$$

By using properties associated with the reciprocal lattice, the previous expression transforms into [23]

$$V_{e-ph}(\mathbf{r}) = \sum_{\mathbf{K},\mathbf{q}} \delta R_{\mathbf{q}} \mathbf{e}_{\mathbf{q}} \cdot (\mathbf{q} + \mathbf{K}) V_{\mathbf{q}+\mathbf{K}} e^{i\,(\mathbf{q}+\mathbf{K})\cdot\mathbf{r}} \tag{A3}$$

where $\mathbf{K}$ are the reciprocal lattice wave vectors, $V_{\mathbf{q}}$ and $\delta R_{\mathbf{q}}$ are the Fourier components of the electron-ion potential and the ion displacement with wave vector $\mathbf{q}$, respectively. $e_{\mathbf{q}}$ is the polarization vector of phonons. Electron transitions in BZ1 only involve the component $\mathbf{K} = 0$, leading to

$$V_{e-ph}(\mathbf{q}) = q \delta R_{\mathbf{q}} V_{\mathbf{q}}. \tag{A4}$$

When $\mathbf{k}'$ remains in BZ1, within the approximation of isotropic bands for phonons, $|\mathcal{M}_{\mathbf{k},\mathbf{k}'}|^2$ reads with $\mathbf{q} = \mathbf{k}' - \mathbf{k}$,

$$\begin{aligned} |\mathcal{M}_{\mathbf{k},\mathbf{k}'}|^2 &= |\langle \varphi_{k'} | V_{e-ph} | \varphi_k \rangle|^2 \\ &= \left| \mathbf{q} \cdot \delta\mathbf{R}_q \, V_q \int d\mathbf{r}\, u_{\mathbf{k}}(\mathbf{r}) u_{\mathbf{k}'}^{\dagger}(\mathbf{r}) \right|^2. \end{aligned} \tag{A5}$$

For transverse phonons, $q\delta R_{\mathbf{q}} = 0$ so that they do not induce any electron transition. To obtain an analytical expression for the longitudinal matrix element ($q\delta R_{\mathbf{q}} \neq 0$), the standard procedure of considering dynamic screening for the ions and static screening for the free electrons is used [5,18,23],

$$\left|\mathcal{M}_{\mathbf{k},\mathbf{k}'}^{L}\right|^2 = \frac{E_{ph}^{L}(q) e^2}{2\varepsilon_0 \varepsilon_c^0 \left(q^2 + q_0^2\right)} \tag{A6}$$

where ε_c^0 is the contribution to the static permittivity of the core electrons and q_0 the static Thomas-Fermi screening wave vector (the associated characteristic distance provides an estimation above which the influence of other electrons is negligible), which reads [5,23]

$$q_0 = \frac{e^2}{\varepsilon_0 \varepsilon_c^0} \sum_{\mathbf{k}} \frac{f(E_k)}{E_k} \tag{A7}$$

with $E_k = \hbar^2 k^2 / 2m_e$ in BZ1. ε_0^c has been set to 6.7 for gold [5]. Within the approximation of free electrons, isotropic dispersion relations, and distribution functions, standard calculations lead to [18]

$$\left.\frac{\partial f(\mathbf{k})}{\partial t}\right|_{e-pt-ph}^{N} = \frac{1}{2\pi\hbar^3}\frac{m_e}{k}\sum_{l,\pm}\int_0^{K/2} dq\, q \left|\mathcal{M}_q^L\right|^2 \overline{J_l^2}\left(\frac{eqF}{m_e\omega^2}\right) \times \left((1-f(k))\, f(k')\left(\frac{1}{2}\pm\frac{1}{2}+n(q)\right) - f(k)\,(1-f(k'))\left(\frac{1}{2}\mp\frac{1}{2}+n(q)\right)\right)\Xi_{\pm} \tag{A8}$$

with $\Xi_{\pm} = 1$ if $((\frac{\hbar q}{2m_e} \pm \frac{E_{ph}}{\hbar q}) + l\frac{\omega_l}{q}) < \frac{\hbar k}{m_e}$ and 0 other while. $E(k') = E(k) \mp E_{ph} + l\hbar\omega$. $\overline{J_l^2}(a) = \frac{1}{2}\int_{-1}^{1} J_l^2(ax)dx$ is the averaged value of the squared Bessel function of order l [33]. The sum over l accounts for absorption and emission of $|l|$ photons depending on the sign of l. Note that when $|\frac{eqF}{m_e\omega^2}| \ll 1$, $\overline{J_0^2}(\frac{eqF}{m_e\omega^2}) \approx 1$, and the contribution of the $l = 0$ term corresponds to the electron-phonon collision operator for relaxation [18].

2. Electron-electron collision

Assuming isotropic distribution functions and static screening, the matrix element reads [5,18,23]

$$|\mathcal{G}_{\mathbf{k}\to\mathbf{k}_2,\mathbf{k}_1\to\mathbf{k}_3}|^2 = \frac{e^4}{\varepsilon_0^4\varepsilon_c^{0\,4}\left(q^2+q_0^2\right)^2} \tag{A9}$$

where $\mathbf{q} = \mathbf{k}_2 - \mathbf{k} = \mathbf{k}_3 - \mathbf{k}_1$. Assuming that electron-electron collisions with parallel spins are negligible [34], a standard procedure to calculate this collision operators leads to [5,43]

$$\left.\frac{\partial f(k)}{\partial t}\right|_{e-e}^{N} = \frac{\pi\hbar}{32m_e}\frac{e^4}{\epsilon_0^2}\frac{1}{E_{TF}\sqrt{E}}\int dE_2 dE_1 \frac{D(E_2)}{k_2}\frac{D(E_1)}{k_1}\left[\frac{\sqrt{\tilde{E}}}{(\tilde{E}+E_{TF})} + \frac{1}{\sqrt{E_{TF}}}\tan^{-1}\left(\sqrt{\tilde{E}/E_{TF}}\right)\right]_{\tilde{E}_{low}}^{\tilde{E}_{up}} \times \left([1-f(k)][1-f(k_1)]f(k_2)f(k_3) + f(k)f(k_1)[1-f(k_2)][1-f(k_3)]\right)|_{E_3=E+E_1-E_2} \tag{A10}$$

where $E_{TF} = \hbar^2 q_0^2/2/m_e$, $\tilde{E}_{up} = \min((\sqrt{E}+\sqrt{E_2})^2; (\sqrt{E_1}+\sqrt{E_3})^2)$, and $\tilde{E}_{low} = \max((\sqrt{E}-\sqrt{E_2})^2; (\sqrt{E_1}-\sqrt{E_3})^2)$. $D(E) = m_e\sqrt{2m_eE}/\pi^2\hbar^3$ is the density of states. $[f(x)]_{x_1}^{x_2} = f(x_2) - f(x_1)$ comes from an integral calculation. Note that the Bessel function accounting for the laser interaction is removed because of the conservation of the total crystalline momentum (the argument of the Bessel function includes K, which is zero). For electron transitions in BZ1, the electron-electron collisions can only induce the relaxation of the electron gas (no photon absorption).

APPENDIX B: SCALING LAW OF Im(ε) WITH THE PHOTON ENERGY

First considering only $e-pt-ph$ normal processes, theoretically, $\mathrm{Im}(\varepsilon)_{e-pt-ph}^{N}$ exhibits the same scaling law as the Drude model, i.e., $\propto 1/\omega^3$ with a constant collision frequency ν_{e-ph} when $\nu_{e-ph} \ll \omega$ [23]. Such result was already explained analytically with a Boltzmann formalism within the condition $k_B T_e \gg \hbar\omega \approx E_F$ [44]. Here we show this result still stands for $k_B T_e \ll E_F$. Considering Eq. (32) for linear normal absorption only, the $e-pt-ph$ collision operator reads

$$\left.\frac{\partial f(\mathbf{k})}{\partial t}\right|_{e-pt-ph}^{N} = \frac{1}{2\pi\hbar^3}\frac{m_e}{k}\sum_{l=\pm1,\pm}\int_0^{K/2} dq\, q \times \left|\mathcal{M}_q^L\right|^2 \frac{1}{12}\left(\frac{e\hbar qF}{m_e\hbar\omega^2}\right)^2 \times \left((1-f(k))\, f(k')\left(\frac{1}{2}\pm\frac{1}{2}+n(q)\right) - f(k)\,(1-f(k'))\left(\frac{1}{2}\mp\frac{1}{2}+n(q)\right)\right)\Xi_{\pm} \tag{B1}$$

with $\Xi_{\pm} = 1$ if $((\frac{\hbar q}{2m_e} \pm \frac{E_{ph}}{\hbar q}) + l\frac{\omega_l}{q}) < \frac{\hbar k}{m_e}$ and 0 other while, $E(k') = E(k) \mp E_{ph} + l\hbar\omega$. Considering $E_{ph} \ll \hbar\omega$ and $T_{ph} \gg \theta_D$ so that $\frac{1}{2} \pm \frac{1}{2} + n(q) = n(q)$, Eq. (B1) reads

$$\left.\frac{\partial f(\mathbf{k})}{\partial t}\right|_{e-pt-ph}^{N} = \sum_{l=\pm1} \nu_{e-ph}^{\mathrm{eff}}(k, l\hbar\omega) \times \left((1-f(k))\, f(k') - f(k)\,(1-f(k'))\right)\frac{1}{12}\left(\frac{e\hbar KF}{m\hbar\omega^2}\right)^2 \tag{B2}$$

where $\nu_{e-ph}^{\mathrm{eff}}(k, l\hbar\omega) = \frac{1}{\pi\hbar^3}\frac{m_e}{k}\int_0^{K/2} dq\, q \times |\mathcal{M}_q^L|^2 \frac{q^2}{K^2} n(q)\Xi$ is a parameter with the dimension of a collision frequency, which only depends on k, $\Xi = 1$ if $\frac{\hbar q}{2m_e} + l\frac{\omega_l}{q} < \frac{\hbar k}{m_e}$ and 0 other while, and $E(k') = E(k) + l\hbar\omega$. Note that collision processes are

mainly due to a phonon with the wave vector of the same order of magnitude as k_F, and with energy of electrons in the vicinity of E_F. Thus, $\Xi = 1$ if $E_F + l\hbar\omega < 2E_F$ and 0 other while. As $\hbar\omega \approx 0.1E_F$, $\Xi = 1$.

The mean power density absorbed by this process finally reads

$$\left.\frac{\partial\langle E\rangle}{\partial t}\right|^{N}_{e-pt-ph} = \left(\frac{e\hbar KF}{m_e\hbar\omega^2}\right)^2 \int dE D(E)E \times \nu^{\text{eff}}_{e-ph}(E)((1-f(E))\, f(E+l\hbar\omega) - f(E)(1-f(E+l\hbar\omega))) \tag{B3}$$

For $k_BT_e \ll E_F$, the product of the electron distribution functions is different from zero only if $|E - E_F| \leqslant \hbar\omega$. Thus, since $\hbar\omega/E_F \approx 0.1$, it is reasonable to assume that $D(E) \times \nu^{\text{eff}}_{e-ph,l}(E) \approx D(E_F)\nu^{\text{eff}}_{e-ph}(E_F)$.

Finally by doing appropriate change of variables, one finally obtains for $k_BT_e \ll E_F$,

$$\left.\frac{\partial\langle E\rangle}{\partial t}\right|^{N}_{e-pt-ph} = \left(\frac{e\hbar KF}{m_e\hbar\omega^2}\right)^2 \nu^{\text{eff}}_{e-ph}(E_F)D(E_F)(\hbar\omega)^2 \propto \frac{F^2}{\omega^2} \tag{B4}$$

identifying $\text{Im}(\varepsilon)$ in Eq (18), we obtain $\text{Im}(\varepsilon)|^{N}_{e-pt-ph} \propto 1/\omega^3$. That explains why despite quantum absorption processes take place, $\text{Im}(\varepsilon)$ follows the same scaling law as the classical Drude model with a constant collision frequency.

[1] M. Bauer, A. Marienfeld, and M. Aeschlimann, Prog. Surf. Sci. **90**, 319 (2015).

[2] L. V. Besteiro and A. O. Govorov, J. Phys. Chem. C **120**, 19329 (2016).

[3] C.-K. Sun, F. Vallée, L. H. Acioli, E. P. Ippen, and J. G. Fujimoto, Phys. Rev. B **50**, 15337 (1994).

[4] M. Zavelani-Rossi, D. Polli, S. Kochtcheev, A.-L. Baudrion, J. Béal, V. Kumar, E. Molotokaite, M. Marangoni, S. Longhi, G. Cerullo *et al.*, ACS Photonics **2**, 521 (2015).

[5] N. Del Fatti, C. Voisin, M. Achenmann, S. Tzortzakis, D. Christofilos, and F. Vallée, Phys. Rev. B **61**, 16956 (2000).

[6] M. Hartelt, P. N. Terekhin, T. Eul, A.-K. Mahro, B. Frisch, E. Prinz, B. Rethfeld, B. Stadtmüller, and M. Aeschlimann, ACS Nano **15**, 19559 (2021).

[7] E. Bévillon, J. P. Colombier, V. Recoules, and R. Stoian, Phys. Rev. B **89**, 115117 (2014).

[8] M. I. Kaganov, I. M. Lifshits, and L. B. Tanatarov, Zh. Eksp. Teor. Fiz. **31**, 232 (1956) [Sov. Phys. JETP **4**, 173 (1957)].

[9] A. M. Brown, R. Sundararaman, P. Narang, W. A. Goddard, and H. A. Atwater, Phys. Rev. B **94**, 075120 (2016).

[10] Y. Petrov, Laser Part. Beams **23**, 283 (2005).

[11] G. V. Hartland, L. V. Besteiro, P. Johns, and A. O. Govorov, ACS Energy Lett. **2**, 1641 (2017).

[12] L. Mascaretti and A. Naldoni, J. Appl. Phys. **128**, 041101 (2020).

[13] S. W. Lee, H. Lee, Y. Park, H. Kim, G. A. Somorjai, and J. Y. Park, Surf. Sci. Rep. **76**, 100532 (2021).

[14] J.-D. Chen, L. Li, C.-C. Qin, H. Ren, Y.-Q. Li, Q.-D. Ou, J.-J. Guo, S.-J. Zou, F.-M. Xie, X. Liu *et al.*, InfoMat **4**, e12285 (2022).

[15] S. Wu, Y. Chen, and S. Gao, Phys. Rev. Lett. **129**, 086801 (2022).

[16] A. M. Brown, R. Sundararaman, P. Narang, W. A. Goddard, and H. A. Atwater, ACS Nano **10**, 957 (2016).

[17] S. Ono, Phys. Rev. B **97**, 054310 (2018).

[18] A. Kaiser, B. Rethfeld, M. Vicanek, and G. Simon, Phys. Rev. B **61**, 11437 (2000).

[19] A. V. Lugouskoy and I. Bray, Phys. Rev. B **60**, 3279 (1999).

[20] A. Blumenstein, E. S. Zijlstra, D. S. Ivanov, S. T. Weber, T. Zier, F. Kleinwort, B. Rethfeld, J. Ihlemann, P. Simon, and M. E. Garcia, Phys. Rev. B **101**, 165140 (2020).

[21] G. Della Valle, M. Conforti, S. Longhi, G. Cerullo, and D. Brida, Phys. Rev. B **86**, 155139 (2012).

[22] J. B. Khurgin, Faraday Discuss. **214**, 35 (2019).

[23] N. Ashcroft and N. Mermin, *Solid State Physics* (Harcourt College Publishers Fort Worth, TX, 1976).

[24] N. Del Fatti, R. Bouffanais, F. Vallée, and C. Flytzanis, Phys. Rev. Lett. **81**, 922 (1998).

[25] J. Seely and E. Harris, Phys. Rev. A **7**, 1064 (1973).

[26] P. Daguzan, Ph.D. thesis, Université Paris, VI 1996.

[27] P. Daguzan, P. Martin, S. Guizard, and G. Petite, Phys. Rev. B **52**, 17099 (1995).

[28] W. V. Houston, Phys. Rev. **57**, 184 (1940).

[29] V. E. Gruzdev, Phys. Rev. B **75**, 205106 (2007).

[30] H. Furuse, N. Mori, H. Kubo, H. Momose, and M. Kondow, Phys. Status Solidi (c) **5**, 286 (2008).

[31] V. Mel'Nikov, ZhETF Pisma Redaktsiiu **9**, 204 (1969).

[32] G. Duchateau, B. Chimier, S. Coudert, E. Smetanina, L. Barilleau, N. Fedorov, H. Jouin, G. Geoffroy, P. Martin, and V. T. Tikhonchuk, Phys. Rev. B **102**, 024305 (2020).

[33] B. Rethfeld, A. Kaiser, M. Vicanek, and G. Simon, Phys. Rev. B **65**, 214303 (2002).

[34] P. J. van Hall, Phys. Rev. B **63**, 104301 (2001).

[35] D. R., *CRC Handbook of Chemistry and Physics* (CRC Press. Boca Raton, Florida, 2003).

[36] S. Babar and J. Weaver, Appl. Opt. **54**, 477 (2015).

[37] P. Nozières and D. Pines, *The Theory of Quantum Liquids* (Perseus Books., Cambridge, Mass., 1999).

[38] J. Khurgin, Nat. Nanotechnol. **10**, 2 (2015).

[39] Z. Lin, L. V. Zhigilei, and V. Celli, Phys. Rev. B **77**, 075133 (2008).

[40] R. Powell, C. Ho, and P. E. Liley, *Thermal Conductivity of Selected Materials* (U.S. Department of Commerce, National Bureau of Standards, 1966).

[41] G. White, Proc. Phys. Soc. A **66**, 559 (1953).

[42] A. Jain and A. J. H. McGaughey, Phys. Rev. B **93**, 081206 (2016).

[43] D. W. Snoke, W. W. Rühle, Y.-C. Lu, and E. Bauser, Phys. Rev. B **45**, 10979 (1992).

[44] W. P. Dumke, Phys. Rev. **124**, 1813 (1961).